













Effector XopQ-induced stromule formation in *Nicotiana benthamiana* depends on ETI signaling components ADR1 and NRG1

Jennifer Prautsch ¹, Jessica Lee Erickson ^{2,3}, Sedef Özyürek ¹, Rahel Gormanns ¹, Lars Franke ⁴, Yang Lu ¹, Jolina Marx³, Frederik Niemeyer ¹, Jane E. Parker ⁵, Johannes Stuttmann ^{2,6} and Martin Hartmut Schattat ^{1,*}

- 1 Biology, Plant Physiology, Martin-Luther-University Halle-Wittenberg, Halle, Germany
- 2 Biology, Plant Genetics, Martin-Luther-University Halle-Wittenberg, Halle, Germany
- 3 Leibniz-Institut für Plant Biochemie, Halle, Germany
- 4 Biochemistry and Biotechnology, Martin-Luther-University Halle-Wittenberg, Halle, Germany
- 5 Max Planck Institute for Plant Breeding Research, Cologne, Germany
- 6 Institute for Biosafety in Plant Biotechnology, Federal Research Centre for Cultivated Plants, Julius Kühn-Institute (JKI), Quedlinburg, Germany

*Author for correspondence: martin.schattat@pflanzenphys.uni-halle.de

J.L.E., J.S., J.E.P., and M.H.S. contributed to experimental design and the written text; J.P., S.Ö., R.G., Y.L., F.N., J.M., and L.F. conducted the *A. tumefaciens* inoculation experiments in *N. benthamiana* and respective image analysis; J.L.E. conducted Xcv inoculation experiments and respective image analysis. The authors responsible for distribution of materials integral to the findings presented in this article in accordance with the policy described in the Instructions for Authors (<https://academic.oup.com/plphys/pages/general-instructions>) are: Martin Hartmut Schattat (martin.schattat@pflanzenphys.uni-halle.de), Jane Parker (parker@mpipz.mpg.de), and Johannes Stuttmann (jstuttmann@gmail.com).

Abstract

In *Nicotiana benthamiana*, the expression of the *Xanthomonas* effector XANTHOMONAS OUTER PROTEIN Q (XopQ) triggers RECOGNITION OF XOPQ1 (ROQ1)-dependent effector-triggered immunity (ETI) responses accompanied by the accumulation of plastids around the nucleus and the formation of stromules. Both plastid clustering and stromules were proposed to contribute to ETI-related hypersensitive cell death and thereby to plant immunity. Whether these reactions are directly connected to ETI signaling events has not been tested. Here, we utilized transient expression experiments to determine whether XopQ-triggered plastid reactions are a result of XopQ perception by the immune receptor ROQ1 or a consequence of XopQ virulence activity. We found that *N. benthamiana* mutants lacking ROQ1, ENHANCED DISEASE SUSCEPTIBILITY 1, or the helper NUCLEOTIDE-BINDING LEUCINE-RICH REPEAT IMMUNE RECEPTORS (NLRs) N-REQUIRED GENE 1 (NRG1) and ACTIVATED DISEASE RESISTANCE GENE 1 (ADR1), fail to elicit XopQ-dependent host cell death and stromule formation. Mutants lacking only NRG1 lost XopQ-dependent cell death but retained some stromule induction that was abolished in the *nrg1_adr1* double mutant. This analysis aligns XopQ-triggered stromules with the ETI signaling cascade but not to host programmed cell death. Furthermore, data reveal that XopQ-triggered plastid clustering is not strictly linked to stromule formation during ETI. Our data suggest that stromule formation, in contrast to chloroplast perinuclear dynamics, is an integral part of the *N. benthamiana* ETI response and that both NRG1 and ADR1 hNLRs play a role in this ETI response.

Introduction

Plastids exhibit exquisite developmental flexibility, as demonstrated by their capacity to differentiate into various plastid types with specialized functions, biochemical activities, and internal structures, depending on the plant organ, developmental stage, or environmental condition. Furthermore, plastids undergo extreme morphological changes, in some cases changing their shape within minutes or seconds (Gunning, 2005; Pyke, 2013; Delfosse et al., 2016). One highly dynamic feature of plastids is the projection of long, stroma-filled tubules formed by the two envelope membranes. These projections, also called stromules, are reliably observed when either the stroma or the envelope membranes are fluorescently labeled (reviewed in Delfosse et al., 2016). Over the last two decades, stromules have been detected by fluorescence microscopy in an increasing number of plant species throughout the *Viridiplantae* (“green plants”; reviewed in Gray et al., 2001), suggesting that stromule formation emerged early during plant evolution. Examination of different plant tissues revealed that while stromule frequencies may vary, stromules are a ubiquitous feature of plastids (Köhler and Hanson, 2000; Holzinger et al., 2008).

Stromules form in response to developmental cues and increase following exposure to various stresses or signaling molecules and metabolites connected to stress (Schattat and Klösgen, 2011b; Gray et al., 2012; Mathur et al., 2012; Caplan et al., 2015; Vismans et al., 2016), suggesting stromule formation is strictly controlled by the plant. These observations led to the hypothesis that stromules participate in processes that are fundamentally important for plant survival during stress, to transmit signals and/or support physiological changes.

Despite their early emergence in the evolution of *Viridiplantae* and their frequent observation across tissues, our knowledge of stromule function is limited. To date, mutants with defects in signaling pathways regulating stromule formation were not identified. Therefore, it remains unclear which processes or functions are carried out by stromules during stress responses and how these might be executed. As an alternative to genetic dissection of stromule formation *per se*, we decided instead to test the effects of mutants in defined stress responses for effects on stromule formation. Our aim is to gain insight into the role of stromules during adaptation to a specific stress and use genetic tools to decipher stromule function.

Biotic stress caused by plant interactions with recognized pathogens results in pronounced stromule formation (Krenz et al., 2012; Erickson et al., 2014; Caplan et al., 2015; Kumar et al., 2018). Many pathogenic microbes transfer virulence factors, known as effectors, into the host cell cytoplasm to promote infection, often by manipulating pattern-triggered immunity (PTI) programs (Toruño et al., 2016; Büttner, 2016). In an incompatible interaction, intracellular immune receptors recognize one or more effectors. Effector recognition triggers a robust immune response termed effector-triggered immunity (ETI), which frequently culminates in

localized host-programmed cell death (a hypersensitive response = HR) at infection sites (Cui et al., 2015; Yuan et al., 2021). Most intracellular immune receptors are nucleotide binding/leucine-rich repeat (NLR) proteins. NLR proteins are represented by two major pathogen-sensing NLR receptor classes, which are defined by their N-terminal domains. The so-called TIR-NLRs (TNLs) possess a Toll/interleukin-1 domain (TIR) and CC-NLRs (CNLs) a coiled-coil (CC) domain at their N-terminus. Additionally, different families of “helper” NLRs (hNLRs) were found to function together with pathogen-detecting (sensor) NLRs (sNLRs) in *Arabidopsis* (*Arabidopsis thaliana*) and solanaceous species, thus connecting sNLRs with downstream immunity factors in ETI (Cui et al., 2015; Wu et al., 2019).

Dramatic increases in stromule frequencies were observed following the expression of effectors recognized by CC-NLRs or TIR-NLRs prior to ETI-induced cell death in *Nicotiana benthamiana* and *Arabidopsis thaliana* (Caplan et al., 2015; Erickson et al., 2018). For example, induction of ETI (resulting in HR) via the transient co-expression of the p50 helicase domain from tobacco mosaic virus and the cognate TIR-NLR immune receptor, N from tobacco (*Nicotiana tabacum*), in *N. benthamiana* results in strong stromule induction (Caplan et al., 2015). Similarly, a screen by our group revealed that the expression of XopQ from the bacterium *Xanthomonas campestris* pv. *vesicatoria* (Xcv; strain 85–10), which is recognized by the TIR-NLR immune receptor RECOGNITION OF XopQ1 (ROQ1) in *N. benthamiana*, also strongly enhanced stromule frequencies (Schultink et al., 2017; Erickson et al., 2018). In the case of ETI activation via N/p50, the authors reported that many stromules were in close proximity to the nucleus, and appeared to make contact. This observation suggested that plastids might directly deliver defense signals to the nucleus via stromules (Caplan et al., 2015; Kumar et al., 2018). Stromule frequency also increased during CC-NLR- and TIR-NLR-mediated ETI in *A. thaliana* when plants were challenged with avirulent strains of the bacterial pathogen *Pseudomonas syringae* (Caplan et al., 2015). Thus, it appears that stromule formation is a common response of plants during ETI.

In addition to an increase in stromule frequencies and stromule-to-nucleus contacts, the formation of plastid clusters around nuclei was observed during ETI responses in *N. benthamiana* (Caplan et al., 2015; Kumar et al., 2018), leading to the conclusion that plastid clusters might also support the delivery of plastid-derived defense signals to the nucleus (Ding et al., 2019; Mullineaux et al., 2020). In time-lapse experiments spanning several minutes (Kumar et al., 2018), plastid bodies moved in the direction of stromule tips/anchor points in the majority of cases, giving the impression that stromules directionally pull the plastid body with them. This observation led to the conclusion that stromules might guide plastids to the nucleus to facilitate clustering. Hence, stromules near the nucleus might have a second function in plastid positioning.

Taken together, ETI-induced stromules present a starting point for more detailed genetic analyses of stromule formation and plastid clustering following the well-defined molecular event of effector recognition. For this, we chose *N. benthamiana* ROQ1-mediated XopQ recognition leading to ETI as a suitable system to critically examine the functional relationship between stromule formation and immunity signaling.

The Arabidopsis immune receptor HopZ-ACTIVATED RESISTANCE 1 (ZAR1), and likely other CNLs, assembles into pentameric resistosome complexes upon activation, which may insert into membranes and function as Ca^{2+} influx channels (Adachi et al., 2019; Bi et al., 2021; Wang et al., 2019a). In contrast, TNLs including ROQ1 were reported to assemble into tetrameric holoenzymes with NADase activity (Ma et al., 2020; Martin et al., 2020), and cannot induce immunity directly. TNL-ETI requires at least two more components: heterodimeric complexes composed of the lipase-like protein ENHANCED DISEASE SUSCEPTIBILITY1 (EDS1) and either PHYTOALEXIN DEFICIENT4 (PAD4) or SENSECENCE-ASSOCIATED GENE101 (SAG101), and hNLRs of the ACTIVATED DISEASE RESISTANCE GENE1 (ADR1) and/or N-REQUIRED GENE1 (NRG1) type. These hNLRs are characterized by an N-terminal CC domain with homology to *A. thaliana* RESISTANCE TO POWDERY MILDEW 8 (RPW8), the so-called CC_R domain, and are therefore referred to as RNLs (Collier et al., 2011; Wagner et al., 2013; Castel et al., 2019; Jubic et al., 2019; Gantner et al., 2019; Lapin et al., 2019; Wu et al., 2019; Saile et al., 2020).

Heterodimeric EDS1 complexes most likely function as receptors for TNL-derived small molecules and are essential for TNL-mediated immune responses in different dicot plants including *A. thaliana* and *N. benthamiana* (Wagner et al., 2013; Gantner et al., 2019; Lapin et al., 2020; Huang et al., 2022; Jia et al., 2022). At least in *A. thaliana*, small molecule binding promotes the formation of EDS1–PAD4–ADR1 and EDS1–SAG101–NRG1 complexes, which can regulate pathogen resistance and cell death, respectively, in TNL immunity (Lapin et al., 2019; Sun et al., 2021). Upon activation, ADR1 and NRG1 RNLs were reported to form a structure similar to the pentameric complex reported for the *A. thaliana* CNL ZAR1 (“resistosome”), which may directly integrate into membranes to function as Ca^{2+} -permeable channels (Wang et al., 2019a, 2019b; Bi et al., 2021; Jacob et al., 2021). In *N. benthamiana*, immune functions are not known for EDS1–PAD4, and an EDS1–SAG101b complex appears to operate mainly through NRG1 to mediate both cell death and resistance in this species (Qi et al., 2018; Gantner et al., 2019; Lapin et al., 2019). *Nicotiana benthamiana* ADR1 immune functions have not been analyzed so far; however, significant XopQ–ROQ1-mediated transcriptional reprogramming in *nrg1* mutant plants (which is completely abolished in *eds1* mutants) in the absence of resistance and cell death suggests that ADR contributes to TNL immunity and that there is some degree of cooperativity or redundancy between the two helper NLR classes in *N. benthamiana* (Qi et al., 2018; Saile et al., 2020).

In this study, we capitalized on the previous characterization of XopQ–ROQ1-induced TNL immunity in *N. benthamiana* and positioned chloroplast stromule formation and perinuclear clustering in downstream signaling networks. Our data suggest that, although stromule formation is tightly linked to immune responses, it can be uncoupled from ETI-triggered cell death. Furthermore, our data support partially redundant functions of the NRG1 and ADR1 hNLRs in stromule formation. Intriguingly, our data indicate that plastid clustering can be largely uncoupled from ROQ1 ETI and hence is unlikely to represent an integral component of the plant’s innate immune response.

Results

Xcv-mediated stromule formation in *N. benthamiana* depends on XopQ

We previously reported that *A. tumefaciens*-mediated transient expression of XopQ from *Xcv* induces stromule formation in *N. benthamiana* (Erickson et al., 2018). During infection with *Xcv* strains such as *Xcv* 85-10, a strain that naturally delivers XopQ to host cells, XopQ is likely less abundant in infected cells than during transient expression experiments. Additionally, XopQ is translocated together with the entire type III-secreted effectome of *Xcv* (>30 effectors; Teper et al., 2016). In order to test the extent to which stromule frequencies measured during transient expression experiments reflect the *Xcv* interaction, different bacterial strains were inoculated into *FNR:eGFP*-expressing transgenic *N. benthamiana* plants. Under our greenhouse conditions, the wild-type strain *Xcv* 85-10 induces an ETI-associated programmed cell death response (indicating XopQ recognition), showing first signs of dead leaf tissue at 2-day post-infiltration (dpi; Adlung et al., 2016). In order to be able to observe plastids in living cells, we collected leaf samples for microscopy 43-h post-inoculation (Figure 1A). To test the role that XopQ and other effectors play in stromule response, *Xcv* mutant strains $\Delta hrcN$ and $\Delta xopQ$ were infiltrated on the same leaf with the wild-type strain. The $\Delta hrcN$ mutant is deficient in type III secretion and serves as a nonvirulent PTI control (Lorenz and Büttner, 2009). $\Delta hrcN$ as well as $\Delta xopQ$ mutant strains of *Xcv* did not induce macroscopically visual changes in infected tissues at 2 dpi and were not distinguishable from the mock infiltration (Figure 1A; Lorenz and Büttner, 2009; Adlung et al., 2016; Adlung and Bonas, 2017). When analyzing the stromule phenotype, treatments differed significantly. The *Xcv* 85-10 strain induced massive stromule induction in the infiltrated tissue. The $\Delta xopQ$ and $\Delta hrcN$ (no effector translocation) mutant-inoculated tissue harbored almost no stromules, with levels comparable to mock inoculations (10-mM MgCl_2 ; see Figure 1B for stromule frequency quantification, Figure 1, C–F as well as Supplemental Figures S1 and S2 for sample images of the microscopic phenotypes and for statistical values Supplemental Table S1).

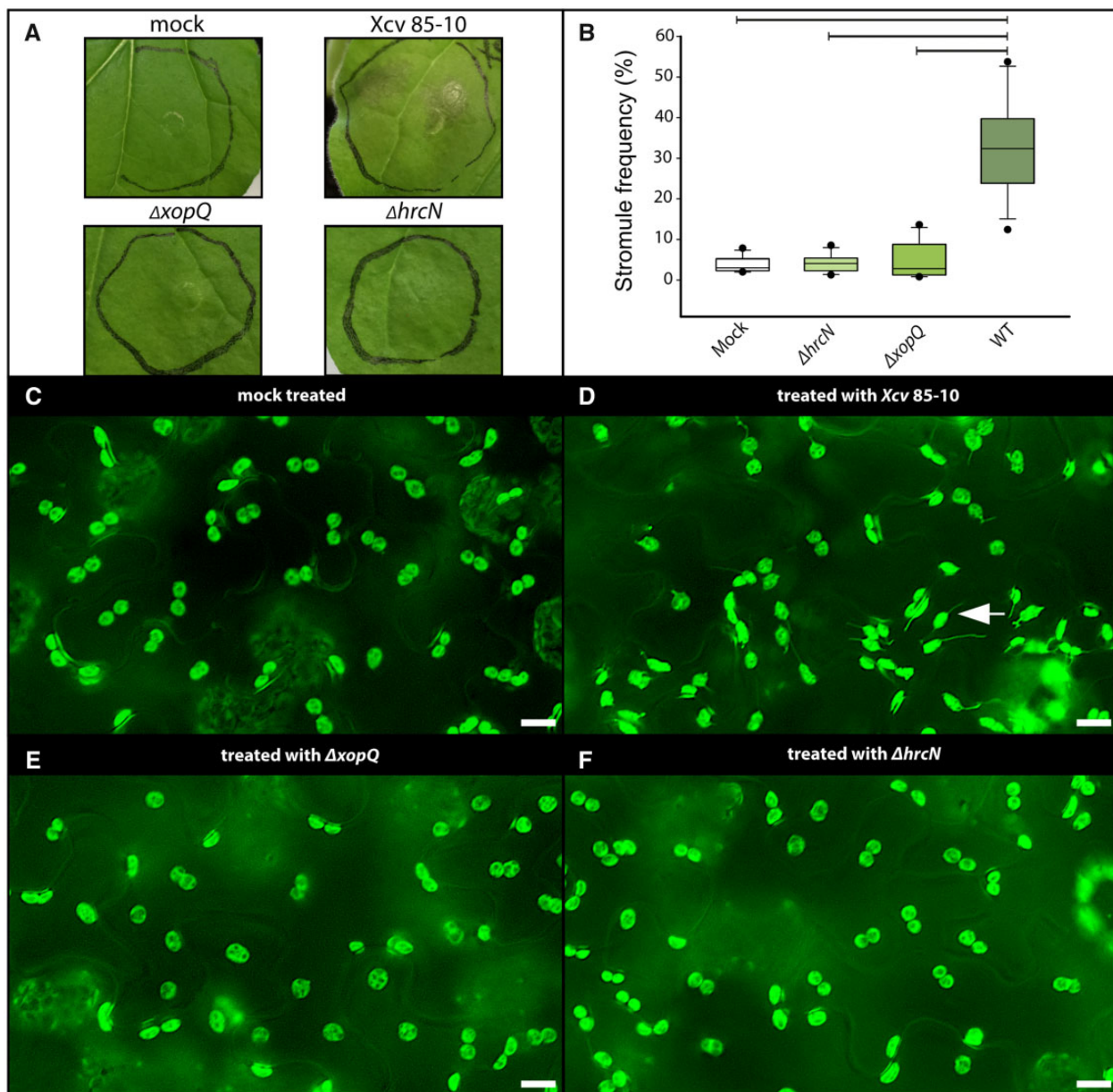


Figure 1 *Xcv* inoculation experiments in wild-type *FNR:eGFP* transgenic plants. A, Macroscopic phenotypes of leaves infiltrated with different *Xcv* strains at 2 dpi. B, Stromule frequency (SF%) of *Xcv*-inoculated tissue at 43-h post-inoculation represented as box plots (box line = median, whiskers = 10th as well as 90th percentile, with each outlier plotted); horizontal lines above bars indicate significantly different stromule frequency values as indicated by a one way analysis of variance (ANOVA) analysis. C–F, Sample sectors of representative microscopic images used for stromule quantification. Fluorescence signals originate from the stably expressed *FNR:eGFP* plastid stroma marker; scale bars = 10 μ m; arrow = stromule (full-frame images shown in Supplemental Figures S1 and S2).

Together with transient expression experiments using *A. tumefaciens* (Erickson et al., 2018), these results indicate that stromule induction at 2 dpi by the *Xcv* wild-type strain is strictly dependent on the presence of XopQ. No other effectors in this strain contributed measurably to stromule induction at 2 dpi when translocated at natural levels. In conclusion, inoculations with *Xcv* strains show that XopQ-triggered stromules appear during pathogen attack at 2 dpi, and supports the idea that stromule induction during transient assays recapitulates a physiologically relevant phenotype.

XopQ fails to induce high stromule frequency values in *roq1* mutant plants

We next examined the extent to which XopQ-triggered stromule induction in the lower epidermis of *N. benthamiana* is a consequence of XopQ perception by the TNL receptor ROQ1, using *A. tumefaciens*-based transient expression. Different *N. benthamiana* mutant lines impaired in XopQ perception or lacking TNL downstream signaling components were co-infiltrated with *Agrobacterium* strains for expression of stroma-targeted eGFP (*SSU:eGFP*) and either *xopQ:mOrange2* or *mOrange2* alone, as control.

Agrobacterium strains were infiltrated at a final optical density $(OD)_{600} = 0.2$, which led to only moderate Agrobacterium-dependent stromule induction ($<20\%$, Erickson et al., 2014) well below XopQ-triggered stromule frequencies ($\sim 60\%$). These experimental conditions were evaluated using *N. benthamiana* stably expressing stroma-targeted eGFP (*FNR:eGFP*; Supplemental Figure S3).

We first tested XopQ-triggered stromule frequencies in *roq1* mutant plants (*roq1-3* and *-4*). ROQ1-deficient plants fail to recognize XopQ and therefore lack the typical ETI-induced yellowing and chlorosis exhibited by wild-type plants following transient XopQ expression (Schultink et al., 2017; Gantner et al., 2019). *xopQ:mOrange2* or the *mOrange2* control were co-infiltrated with a stroma-targeted GFP (*SSU:eGFP*) into wild-type and mutant plants to allow for the visualization of plastids and stromules. As a control for XopQ recognition, macroscopic phenotypes of the co-infiltrated leaves were recorded at 10 dpi, a time point when symptoms are clear despite the low optical densities used for infiltration (Figure 2A). As expected, *xopQ:mOrange2* expression in wild-type plants resulted in chlorosis of the infiltration spot, indicative of the XopQ-triggered ETI response (Adlung et al., 2016). In *roq1-3* and *roq1-4* plants, there was no visible chlorosis, and tissues were indistinguishable from control infiltrations. In all plant lines, *mOrange2* controls showed stromule frequency values characteristic of leaves infiltrated with “empty” GV3101 (pMP90) bacteria (compare Figure 2B with Supplemental Figure S3), indicating that the *roq1* mutation does not alter basal stromule frequencies. Compared to *mOrange2*, *xopQ:mOrange2* expression resulted in significantly higher stromule induction in wild-type plants, as previously described (Erickson et al., 2018). In contrast, *xopQ:mOrange2* expression failed to induce stromules beyond GV3101 (pMP90) basal levels in the *roq1-3* and *roq1-4* mutant plants (Figure 2B; Supplemental Table S2). Average stromule frequencies in mutants expressing *xopQ:mOrange2* were equal to or less than *mOrange2* controls. While mORANGE2 accumulates in the cytoplasm as well as in the nucleoplasm the fusion protein XopQ-mORANGE2 accumulates only in the cytoplasm (Figure 2, C–F; for full frame images, see Supplemental Figures S4 and S5). The full loss of XopQ-triggered stromule formation in *roq1* mutant plants shows that XopQ recognition by ROQ1 is required for stromule induction and that nonrecognized XopQ activity does not generate a stromule-inducing signal.

XopQ–ROQ1-dependent stromule induction requires EDS1

EDS1 is essential for resistance and cell death mediated by TNL-type immune receptor ROQ1 (Adlung et al., 2016; Gantner et al., 2019). In order to test if XopQ-triggered stromule formation is dependent on EDS1, co-infiltrations were repeated in *eds1a-1* knockout and wild-type plants. With respect to stromule frequency and macroscopic phenotype, the wild-type plants responded as seen in previous

experiments (Figure 3, A and B; Supplemental Table S2). In contrast, the wild-type *eds1a-1* plants did not show signs of chlorosis at 10 dpi in response to *xopQ:mOrange2* expression, which is consistent with literature reports (Figure 3A; Adlung et al., 2016; Gantner et al., 2019). As was the case for *roq1* mutant plants, XopQ-triggered stromules were not observed in *eds1a-1* tissues (Figure 3, C–F; for full frame images, see Supplemental Figure S6 and Supplemental Table S2). These results indicate that stromule formation in response to XopQ occurs downstream of EDS1 signaling, suggesting that XopQ–ROQ1 interaction and ROQ1 tetramerization (“resistosome” formation; Schultink et al., 2017; Martin et al., 2020) are not sufficient to induce stromules.

XopQ-triggered stromule induction depends on RNLs but is not a consequence of host cell death

In *A. thaliana*, RNL-type NLRs of the ADR1 and NRG1 subfamilies contribute to TNL immunity (Castel et al., 2019; Lapin et al., 2019; Wu et al., 2019; Saile et al., 2020). In *N. benthamiana* *nrg1* mutant plants, resistance and cell death induced by several TNLs was fully abolished, suggesting NRG1 as the major RNL in TNL immunity in this species (Qi et al., 2018). To test if XopQ-triggered stromule formation is NRG1-dependent, two mutant lines with different genomic deletions, *nrg1-4* and *nrg1-5* (Ordon et al., 2021), were analyzed. The *nrg1* mutants did not show signs of yellowing in response to *A. tumefaciens*-mediated XopQ expression, and infiltration spots were macroscopically indistinguishable from control infiltrations (Figure 4A), as expected (Qi et al., 2018; Ordon et al., 2021). All three plant lines responded similarly to the *mOrange2* control expression, with stromule frequencies reaching approximately 25% (Figure 4B; Supplemental Table S2). In contrast, the response to *xopQ:mOrange2* was markedly different between wild-type and *nrg1* mutant lines (Figure 4B). *xopQ:mOrange2* expression in the *nrg1* background induced stromule frequencies values which were intermediate between *mOrange2* and *xopQ:mOrange2* expressing wild-type plants (Figure 3, C–F; for full frame images see Supplemental Figure S7). Although *roq1*, *eds1*, and *nrg1* mutants were equally deficient in XopQ-triggered cell death (necrosis), stromule formation did not strictly require NRG1 and is thus uncoupled from NRG1-mediated cell death. In support of this notion, the transient overexpression of NRG1 under the control of the native promoter (*pNRG1*) in *FNR:eGFP* plants failed to induce cell death, but significantly induced stromule formation (Supplemental Figure S8). This was in contrast to NRG1 under the control of mannopine synthase or ubiquitin promoter fragments, which resulted in strong cell-death phenotypes (Supplemental Figure S9A).

So far, a function of ADR1 was not identified in *N. benthamiana* but varied contributions of these RNLs to Arabidopsis TNL ETI suggested that *N. benthamiana* ADR1 might steer residual stromule formation in *N. benthamiana* *nrg1* lines (Lapin et al., 2019; Saile et al., 2020; Sun et al.,

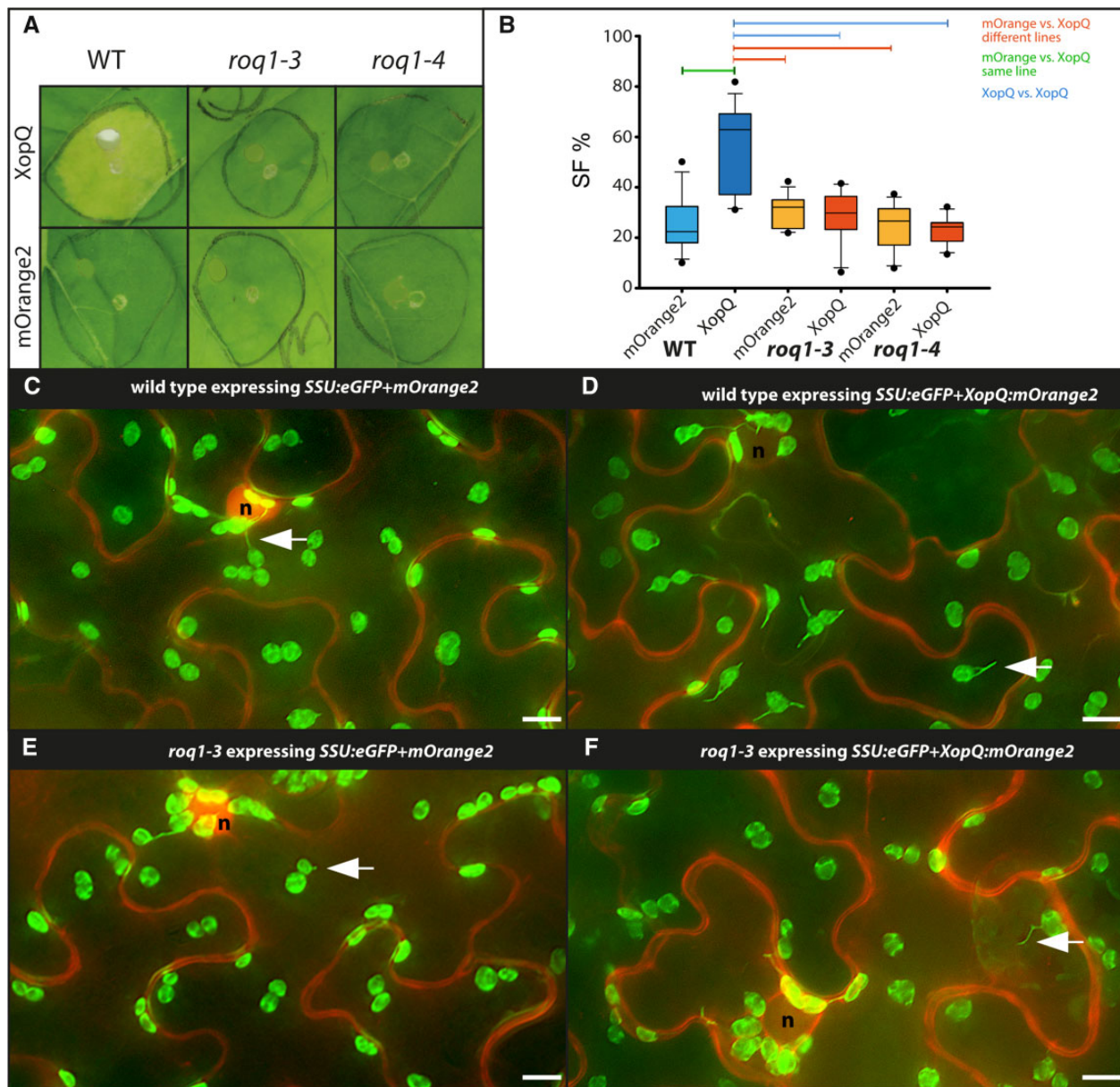


Figure 2 Test for XopQ-mediated stromule formation in lower leaf epidermis cells of *roq1* mutants (*N. benthamiana*). A, Macroscopic phenotypes of Agrobacterium-mediated *xopQ:mOrange2* and *mOrange2*-expression in wild-type, *roq1-3*, and *roq1-4* leaves 10 dpi. B, Results of stromule quantification expressed as stromule frequency (SF%) represented as box plots (box line = median, whiskers = 10th as well as 90th percentile, with each outlier plotted); horizontal lines above bars indicate significantly different stromule frequency values as indicated by a one-way ANOVA analysis. C–F, Sample sectors of representative microscopic images used for stromule quantification. Plastid localized fluorescence originates from the *SSU:eGFP* plastid stroma marker; cytosolic fluorescence originates from the mORANGE2 fluorescence protein (C and E = *mOrange2* controls; d and f *mOrange2* fused to *xopQ*); nuclei = “n”; arrow = stromule; scale bars = 10 μ m. (full-frame images shown in Supplemental Figures S4 and S5).

2021). Therefore, we tested stromule formation in response to XopQ in a recently generated *adr1_nrg1* double mutant line using co-infiltrations as before. As in the *nrg1* single mutants, *xopQ:mOrange2* expression did not induce yellowing or cell death in *adr1_nrg1* plants (Figure 5A). In contrast to our observations in *nrg1* single mutants, *xopQ:mOrange2* did not induce the formation of stromules beyond the *mOrange2* control in *adr1_nrg1* plants (see Figure 5B for box plots and Figure 5, C–F for representative images; for full frame images, see Supplemental Figure S9; for statistical

values, see Supplemental Table S2). Accordingly, the *adr1_nrg1* mutant exhibited stromule and cell death phenotypes similar to the *roq1* (Figure 2A) and *eds1* (Figure 3A) mutant lines. Overall, these results show that not only NRG1 but also ADR1 contributes to stromule formation in *N. benthamiana*. Hence, these results uncover that the ADR1 family of RNLs exhibits not only ETI signaling functions in *A. thaliana* ETI but, at least in the absence of NRG1, also functions in the ETI response of *N. benthamiana* plants.

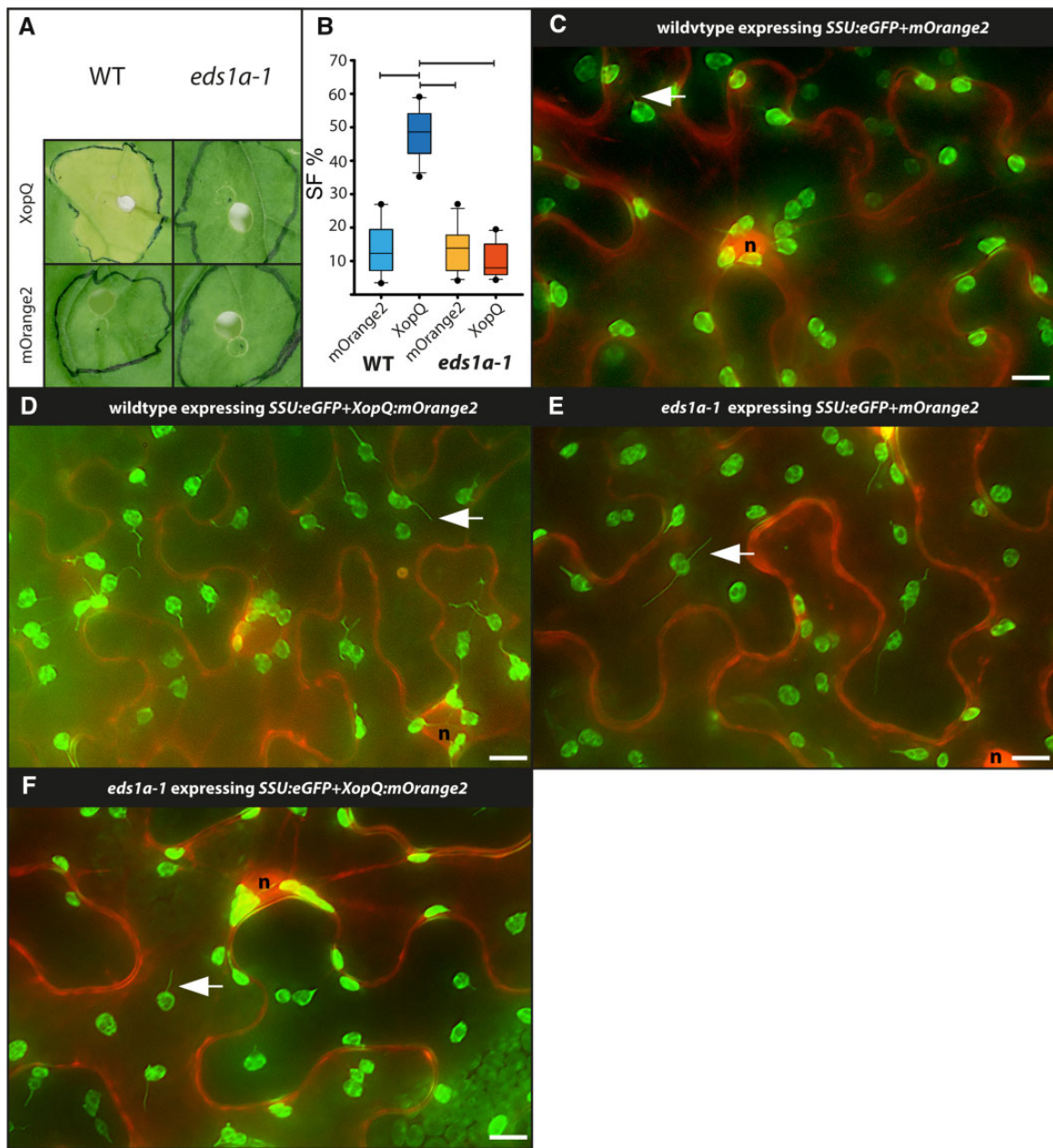


Figure 3 Test for XopQ-triggered stromule formation in the lower leaf epidermis of *eds1a-1* mutants (*N. benthamiana*). A, Macroscopic phenotypes of *xopQ:mOrange2* and *mOrange2* infiltrated wild-type and *eds1a-1* leaves at 10 dpi. B, Results of stromule quantification expressed as stromule frequency (SF%) represented as box plots (box line = median, whiskers = 10th as well as 90th percentile, with each outlier plotted); horizontal lines above bars indicate significantly different stromule frequency values as indicated by a one-way ANOVA analysis. C–F, sample sectors of representative microscopic images from the data set used for stromule quantification. Plastid localized fluorescence originates from the *SSU:eGFP* plastid stroma marker; cytosolic fluorescence originates from the *mORANGE2* fluorescence protein (C and E *mORANGE2*; D and F *mORANGE2* fused to *XopQ*); nuclei = “n”; arrow = stromule; scale bars = 10 μ m (full-frame images shown in Supplemental Figure S6.)

XopQ-triggered perinuclear plastid clustering does not require TNL immune signaling

In order to test if XopQ-triggered ETI facilitates the formation of chloroplast clusters, and whether this has the same genetic dependencies as found for stromule frequencies, chloroplast clustering was quantified in wild-type, *roq1-3*, *eds1a-1*, *nrg1-4*, and *adr1_nrg1* lines. As a measure for plastid clustering, the number of plastids in close proximity (up to one plastid in diameter) to the nucleus was counted and

expressed as the plastid–nucleus association index (PNAI; see Erickson et al., 2014, 2018). In these experiments, *mORANGE2* or *XopQ-mORANGE2* fluorescence, respectively, served to highlight the position of nuclei (see Figure 6, B–K). In control infiltrations (*mOrange2*), wild-type and all four mutants produced similar numbers of plastids around the nucleus (Figure 6A; Supplemental Table S3); no significant differences in PNAI were detected. When challenged with XopQ, plastid clustering increased in wild-type

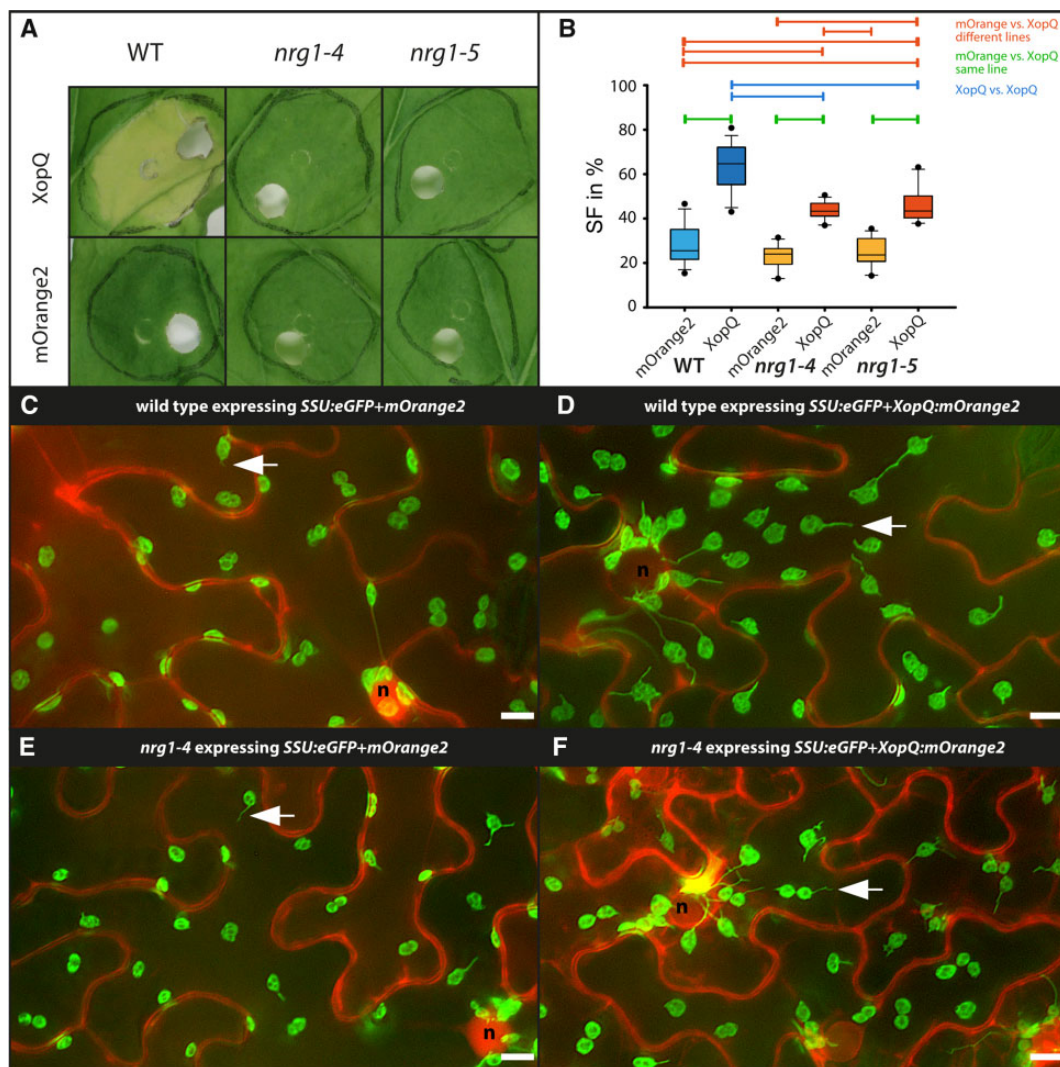


Figure 4 Test for XopQ-mediated stromule formation in lower leaf epidermis cells of *nrg1* mutants (*N. benthamiana*). A, Macroscopic phenotypes of *XopQ:mOrange2* and *mOrange2*-expressing wild-type, *nrg1-4* and *nrg1-5* leaves at 10 dpi. B, Results of stromule quantification expressed as stromule frequency (SF%) represented as box plots (box line = median, whiskers = 10th as well as 90th percentile, with each outlier plotted); horizontal lines above bars indicate significantly different stromule frequency values as indicated by a one-way ANOVA analysis. C–F, Sample sectors of representative microscopic images used for stromule quantification. Plastid localized fluorescence originates from the *SSU:eGFP* plastid stroma marker; cytosolic fluorescence originates from the *mORANGE2* fluorescence protein (C and E = *mOrange2* control; d and f = *mOrange2* fused to *XopQ*); nuclei = “n”; arrow = stromule; scale bars = 10 μ m. (full-frame images shown in Supplemental Figure S7).

plants (Figure 6A; Supplemental Table S3). Although plastid clustering has been considered an ETI response (Caplan et al., 2015; Kumar et al., 2018; Ding et al., 2019), we found that XopQ-triggered plastid clustering was not diminished in mutant lines impaired in XopQ recognition or downstream signaling (Figure 6A; Supplemental Table S3). Upon expression of *xopQ:mOrange2*, *nrg1-4* plants showed wild-type levels of plastid clustering, while *eds1* and *adr1_nrg1* mutants actually had significantly higher PNAI values (Figure 6A; Supplemental Table S3). Figure 6, B–K shows representative images of the different plant lines expressing *SSU:eGFP + xopQ:mOrange2* or *SSU:eGFP + mOrange2*. This is further supported by the *NRG1* over-expression experiments (Supplemental Figure S9) where despite the induction of stromules, *pNRG1::NRG1* expression does not increase PNAI

values; as would be expected if *NRG1*-dependent signaling events contribute to perinuclear plastid clustering.

We concluded that when the XopQ-triggered ETI signal cascade is blocked (*roq1*, *eds1*, and *adr1_nrg1* mutants), the tendency of plastids to cluster around the nucleus remains, and is even enhanced compared to wild-type plants or the *nrg1* line with residual ETI signaling (Figure 6H). These data suggest that one feature of *ROQ1*–XopQ-triggered ETI is suppression of plastid clustering.

Discussion

Here, we set out to understand how ETI-associated stromule formation aligns with signaling processes downstream of immune receptor activation, using recognition

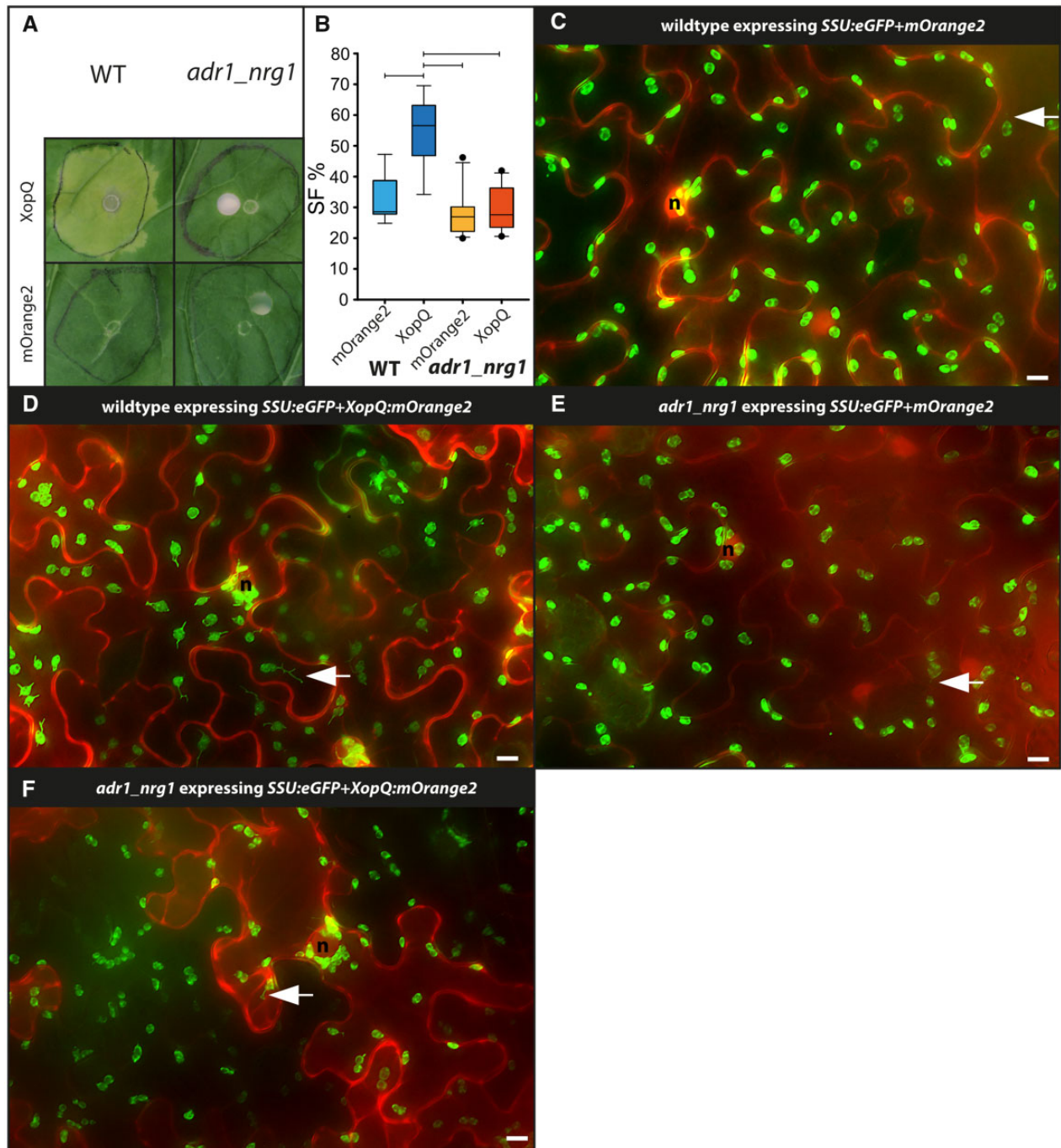


Figure 5 Test for XopQ mediated stromule formation in lower leaf epidermis cells of *adr1_nrg1* double mutants (*N. benthamiana*). A, Macroscopic phenotypes of *xopQ:mOrange2* and *mOrange2*-infiltrated wild-type and *adr1_nrg1-5* leaves at 10 dpi. B, Results of stromule quantification expressed as stromule frequency (SF%) represented as box plots (box line = median, whiskers = 10th as well as 90th percentile, with each outlier plotted); horizontal lines above bars indicate significantly different stromule frequency values as indicated by a one-way ANOVA analysis; wild-type three plants and *adr1_nrg1* five plants for each of three repeats. C–F, Cropped images used for stromule quantification. Plastid localized fluorescence originates from the *SSU:eGFP* plastid stroma marker; cytosolic fluorescence originates from the *mORANGE2* fluorescence protein (C and E are *mOrange2* controls; d and f show *mOrange2* translation fusion with *XopQ*); nuclei = "n"; arrow = stromule; scale bars = 10 μ m (full-frame images shown in Supplemental Figure S8).

of the effector XopQ by the TNL ROQ1 in *N. benthamiana* as a case study. A quantitative analysis of stromule formation and perinuclear plastid clustering in XopQ recognition and ETI signaling mutants produced several

important insights. First, complete absence of a XopQ-related stromule response in *roq1* and *eds1* mutants shows that XopQ-triggered stromules are not a result of its virulence/effector activity, but result from effector

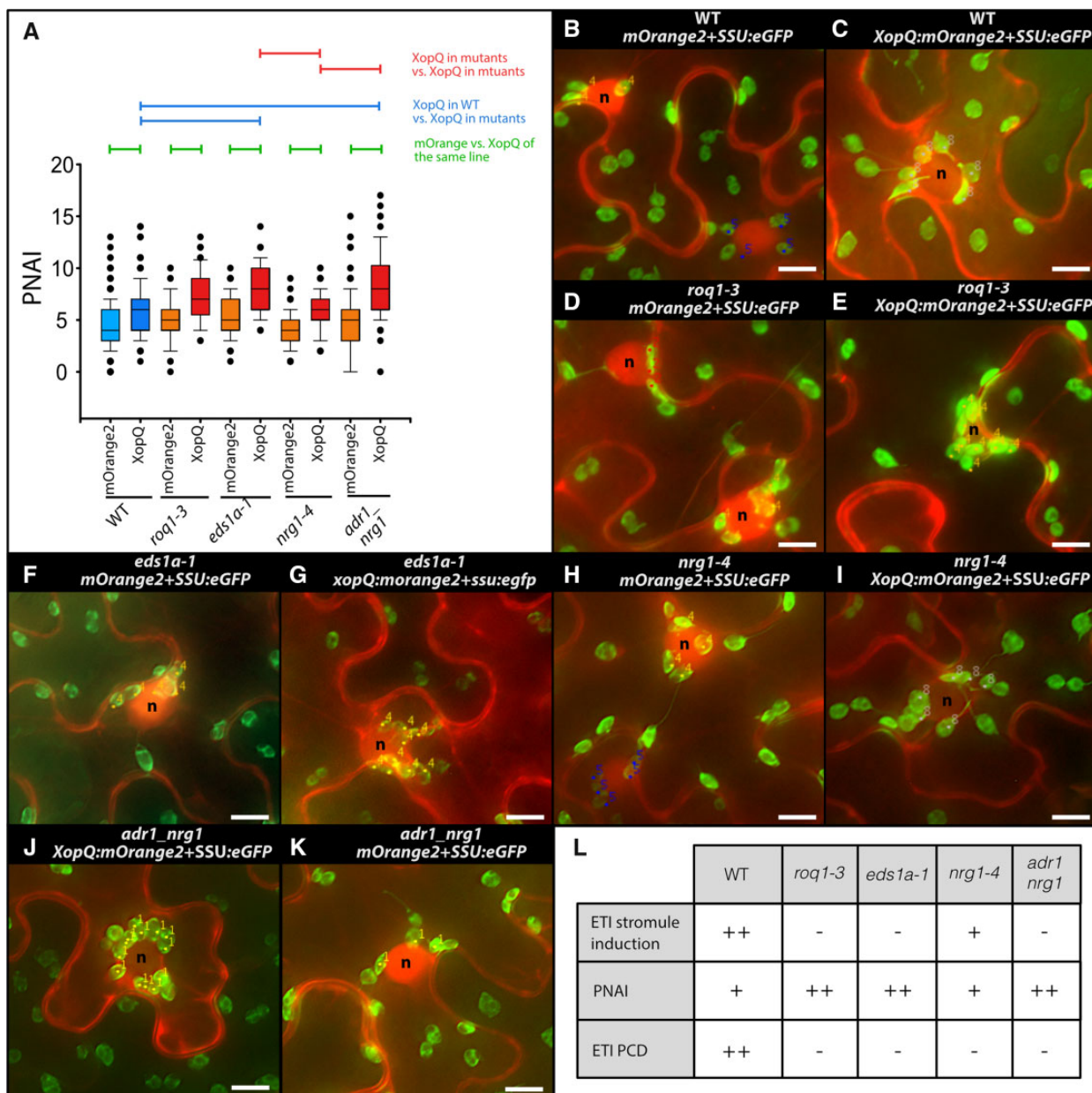


Figure 6 PNAI—Analysis of plastid clustering in response to XopQ expression (*N. benthamiana*). PNAI at 3 dpi following *mOrange2* and *xopQ:mOrange2* expression in wild-type as well as mutant plant lines (*roq1-3*, *eds1a*, *nrg1-4*, and *adr1_nrg1*). A, PNAI values represented in box plots (box line = median, whiskers = 10th as well as 90th percentile, with each outlier plotted); horizontal lines above box plots indicate significantly different stromule frequency values as indicated by a one-way ANOVA on ranks analysis. B–K, Sample images of nuclei with associated plastids (labeled with a dot a number as they were during original plastid scoring); “n” = nuclei; scale bars = 10 μ m. L, Summary of observed ETI stromule, PNAI and cell death phenotypes where “–” = no change compared to control, “+” = visible but moderate increase; “++” = strong increase.

recognition by the ROQ1 immune receptor and a resulting *EDS1*-dependent ETI response. Second, residual induction of stromules in the *nrg1* mutant in the absence of macroscopic cell death suggests that induced stromule formation is not a consequence of NRG1-mediated host cell death but is more closely related to ETI signaling. Third, analysis of the *nrg1_adr1* double mutant line reveals that residual XopQ-triggered ETI and stromule frequency in *nrg1* (but not *eds1*) is conferred by ADR1 in

N. benthamiana. This reveals an ADR1 contribution to TNL ETI processes in a solanaceous plant in the absence of NRG1, suggesting usage of both RNLs NRG1 and ADR1 branches in ETI, as observed in *A. thaliana*. Finally, ROQ1-XopQ-triggered plastid clustering does not relate to ETI induction and stromule formation and is thus likely to be a direct or indirect consequence of XopQ virulence activity during infection. A model summarizing these findings is presented in Figure 7, A and B.

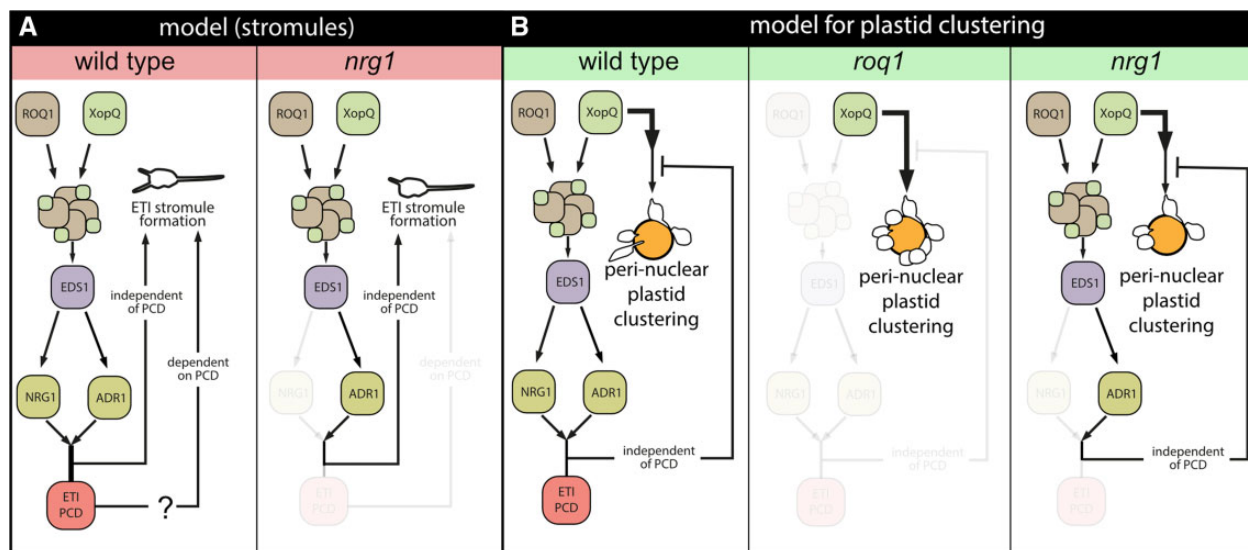


Figure 7 Model of XopQ-mediated stromule induction and perinuclear plastid clustering. A, Model for ETI-induced stromule formation by XopQ in wild-type plants (left): XopQ (*Xanthomonas outer protein Q*) is recognized by the TIR-NB-LRR (TOLL INTERLEUKIN 1 RECEPTOR NUCLEOTIDE-BINDING LEUCINE-RICH REPEAT) resistance protein ROQ1 (RECOGNITION OF XopQ 1), which forms with XopQ a heteromeric protein complex, the so-called “resistosome”. From the “resistosome”, the information of XopQ recognition is transferred with the help of EDS1 to the RNL class helper NLRs NRG1 and ADR1, which culminates in programmed cell death (PCD) as well as stromule formation. In *nrg1* mutants (right), XopQ fails to induce cell death but at the same time still shows significant ETI stromule induction mediated most likely by ADR1. This indicates the existence of a PCD-independent ETI stromule induction pathway. However, at this point, a role for PCD in stromule induction or a role for stromules in PCD is not ruled out (?). B, Model for perinuclear plastid clustering following *xopQ* expression: In wild-type plants (left), an intact ETI signal chain partially suppresses the strong perinuclear plastid clustering induced by XopQ presence. When ETI signal transduction is blocked (*eds1*, *roq1*, and *adr_nrg1* mutants) this suppression does not take place and plastid clustering is enhanced (middle). The restricted ETI signal chain in *nrg1* mutants (right) is sufficient for suppression of induced perinuclear plastid clustering to wild-type levels, thus suppressing signals likely originate from this pathway. Both models only consider genes, which were analyzed as part of this study. The role of the different proteins forming distinct complexes with EDS1 will have to be elucidated in the future.

Uncoupling immune signaling and HR-induced stromules

Stromules have been proposed to transmit retrograde signals to the nucleus, and to amplify programmed cell death responses as part of ETI (Caplan et al., 2015). More recently, it was suggested that stromules have the added function of locating and pulling plastid bodies to the nucleus (Kumar et al., 2018). So far, all reported microbial effectors that induce stromules also provoked programmed cell death (Caplan et al., 2015; Erickson et al., 2018). Therefore, it remained unclear whether stromule formation accompanies the cascade of events contributing to host cell death or is a by-product of physiological changes in cells as they die. The observed stromule induction upon XopQ expression in *nrg1* mutant plants without cell death or measurable resistance (Qi et al., 2018) (Figure 5A) suggests stromules represent events upstream of ETI-related pathogen resistance and host cell death. This is supported by clear stromule induction and simultaneous lack of cell death in response to *pNRG1::NRG1* expression in wild-type plants expressing *FNR:eGFP* (see Supplemental Figure S9, A–H). Hence, ETI-induced stromule formation is not coupled to cellular destruction but is more likely an integral part of the ETI response, as suggested previously (Caplan et al., 2015).

ADR1 contributes to TNL immunity and stromule formation in *N. benthamiana*

Dicot genomes encoding TNL receptors generally also encode RNL-type NLRs of the ADR1 and NRG1 classes (Collier et al., 2011; Lapin et al., 2020). In *A. thaliana*, both classes of RNLs contribute to immunity to different extents. Three *A. thaliana* ADR1 putative paralogs have functions in basal immunity to virulent pathogens related to salicylic acid, and they also contribute to PTI (Bonardi et al., 2011; Jubic et al., 2019; Pruitt et al., 2021; Tian et al., 2021). ADR1s and NRG1s function in *A. thaliana* as distinct modules, respectively, with EDS1–PAD4 and EDS1–SAG101 dimers regulating pathogen resistance and cell death (Lapin et al., 2019; Lapin et al., 2020; Saile et al., 2020; Sun et al., 2021). In *N. benthamiana*, only EDS1–SAG101 appears to execute TNL ETI, and NRG1 was identified as a major RNL required for cell death and resistance mediated by several tested TNLs (Qi et al., 2018; Gantner et al., 2019). A role for *N. benthamiana* ADR1 in immunity was so far not detected, although Qi et al. (2018) reported residual transcriptional reprogramming occurring upon ROQ1 activation in *nrg1*, but not *eds1* mutant plants. Notably, ADR1 was among the upregulated genes of an *NRG1*-independent regulon (Qi et al., 2018). Residual stromule formation in *nrg1*, but not *eds1* or

nrg1_adr1 (compare panel “(A)” in Supplemental Figures S4, S5, and S6), supports an ADR1 contribution to TNL-ETI in *N. benthamiana*. Hence, stromule formation appears to be a highly sensitive read-out for ETI induction, occurring in the absence of cell death or measurable pathogen resistance which are blocked in *N. benthamiana nrg1* and *eds1* mutants (Qi et al., 2018). Current evidence suggests that RNLs, similar to the CNL ZAR1, can assemble into pore-forming resistosome complexes and function as Ca^{2+} permeable cation channels (Wang et al., 2019a; Jacob et al., 2021; Bi et al., 2021). Induced Ca^{2+} influx into host cells would then amplify ROS generation and salicylic acid signaling as well as transcriptional reprogramming (Lu and Tsuda, 2021; Yuan et al., 2021). In future work, it will be interesting to examine whether Ca^{2+} levels inside cells influence stromule formation, as stromule-to-nucleus connections were found to contribute to ROS formation (Caplan et al., 2015).

Perinuclear plastid clustering is independent of ETI stromule induction

In an emerging concept, plastids are the source of important immune response signaling and defense metabolites, including precursors of salicylic acid and jasmonic acid. Many plastid-derived signals must reach the nucleus to fulfill their proposed functions (reviewed in Kretschmer et al., 2020). Thus, re-localization of plastids toward the nucleus might promote more efficient signal transmission. Indeed, when challenged with different pathogens and H_2O_2 , plastids relocated toward the nucleus in *N. benthamiana* epidermis leaf cells, forming perinuclear clusters (Erickson et al., 2014; Caplan et al., 2015; Ding et al., 2019a). How plant cells regulate the re-localization of plastids to the nucleus upon different stimuli remains unknown. Based on the observations of stromule orientation often coinciding with plastid directional movement, it was proposed that stromules are initiated during ETI and extend along the microtubules network, finding anchor points on actin filaments close to the nucleus which guide plastid body movement toward nuclei (Kumar et al., 2018). Perinuclear plastid clustering, as a consequence, might enhance plastid-to-nucleus signal transfer underpinning immune responses. When we challenged wild-type plants with XopQ-mORANGE2, stromule formation as well as perinuclear plastid clustering were consistently induced in lower epidermis cells (Figure 6, A–K). Additionally, stromules facing the nucleus and seemingly anchored in the nuclear periphery were observed (see Figures 2, B, 3, B, 4, B, and 5, B for SF%; e.g. 2D, 3D, and 4D for nucleus-associated stromules). Both observations support stromules guiding plastid body movement (Kumar et al., 2018). However, based on this model we expected impaired or abolished perinuclear clustering in plant lines unable to recognize XopQ (*roq1*) or to initiate TNL downstream signaling (*eds1*, *nrg1*, *nrg1_adr1*). Despite having reduced numbers of ETI-associated stromules, the plastid clustering still occurred when *xopQ:mOrange2* was expressed in respective mutant backgrounds. Notably, plastid clustering was more

pronounced in the mutants compared to the wild-type. In contrast, perinuclear clustering in response to *xopQ:mOrange2* expression was not reduced in *nrg1* plants (Figure 6, A–K) or upon expression of *pNRG1::NRG1* in wild-type plants (Supplemental Figure S9C). In summary, we observe a negative association between stromule frequency and perinuclear plastid clustering. Accordingly, in our assays, ETI induction of stromules was associated with lower plastid clustering compared to when ETI was disabled (Figure 6H). These data suggest that perinuclear plastid clustering is not facilitated by ETI-induced stromules, but instead might be due to other mechanisms, which are enhanced by XopQ virulence activity.

Is induction of perinuclear plastid clustering a part of XopQ's function?

Stronger plastid clustering observed in the absence of ROQ1, EDS1, and ADR1 together with NRG1 RNLs suggests it may represent a consequence of undisturbed XopQ activity (Figures 6, A and 7, B). This observation partially contradicts the suggestion that perinuclear plastid clustering supports ETI responses by facilitating more efficient transfer of pro-defense signals from plastids to the nucleus (discussed in Mullineaux et al., 2020). If the sole function of perinuclear plastids is to enhance ETI, why should the bacteria facilitate perinuclear plastid clustering via XopQ in the absence of effector recognition? Conversely, why suppress clustering when ETI is induced by XopQ? Our results suggest that clustering may serve multiple functions or is the consequence of several stimuli in plant–pathogen interactions. In support of this hypothesis, while plastid clustering in *N. benthamiana* occurs in response to ETI-triggering stimuli (e.g. TMV-p50 and AvrRpt2 recognition Kumar et al., 2018; Ding et al., 2019), it also occurs in response to PTI stimuli (*Pst* DC3000 Δ *hopQ1-1*, *flg22* and H_2O_2 , Ding et al., 2019), which demonstrates that plastid clustering is not ETI specific. Additionally, plastid clustering is not restricted to plant–microbe interactions and has been found to be important for plastid inheritance during cell division (Sheahan et al., 2004, 2020) and has been observed following the exposure of *N. benthamiana* epidermis leaf cells to cytokinin (Erickson et al., 2014). In summary, although plastid accumulation at the nucleus is linked to plant–microbe interactions, it is not exclusively so and may reflect one output resulting from changes to different cell physiological parameters (i.e. altered hormone or H_2O_2 levels). Currently, although we see that XopQ activity induces clustering, the trigger for this phenotype remains enigmatic and it remains to be seen whether it is of any benefit to *Xcv* during an infection.

Does PTI play a role in the phenotypes observed in response to XopQ expression?

Hormone-triggered expression of effectors from transgenes, as recently developed by Ngou et al. (2020), allows for the induction of ETI responses without simultaneously triggering PTI via PAMPs derived from bacterial infiltration. This

approach revealed that despite separate early signaling components, PTI and ETI signaling partially converge further downstream, resulting in similar outputs, suggesting PTI and ETI signaling crosstalk (reviewed in Yuan et al., 2021). Since the system chosen for this study utilizes *A. tumefaciens* to mediate protein expression, the ETI-induced phenotypes observed are always occurring in the presence of a basal immune response to the bacteria, as would be the case during an encounter with a pathogen. However, in the future using the stable inducible transgenic system described by Ngou et al. (2020) in EDS1-dependent signaling mutants will allow for the evaluation of the importance of PTI to XopQ-triggered responses described here.

Conclusion

The goal of this study was to test if stromule formation in response to XopQ-triggered ETI is merely the consequence of cell death and if XopQ-triggered stromules support perinuclear plastid clustering. Here we provide experimental evidence for a direct link between ETI-signal induction and stromule formation, supporting the hypothesis of Caplan et al. (2015), which suggests that stromules play a specific role during ETI. Our findings therefore encourage the enquiry of the nature of this specific role in the future. In contrast to this, our results do not support the second hypothesis, which suggested that stromules might be needed to guide plastid movement toward the nucleus (Kumar et al., 2018), highlighting the fact that there is currently no mechanistic explanation for perinuclear plastid accumulation and that an explanation for this phenomenon will require further investigation. Additionally, residual stromule formation in *nrg1*, but not *adr1_nrg1* double mutant plants, suggests that stromules are a highly sensitive read-out for low-level ETI responses in the absence of resistance and cell death.

Materials and methods

Plant material

Nicotiana benthamiana plant lines used in this study were: wild-type, *roq1-3*, and *roq1-4* (Gantner et al., 2019), *eds1-1* (also referred to as *eds1a-1*; Ordon et al., 2017), *nrg1-4* and *nrg1-5* (Ordon et al., 2021). An *adr1_nrg1* double mutant was created by genome editing using a derivative of pDGE311, a plant transformation vector containing additional counter-selection markers and an intron-optimized *zCas9i* gene, as recently described (Grützner et al., 2021; Stuttmann et al., 2021) (Supplemental Materials and Methods S1). For *Xanthomonas* inoculations transgenic *N. benthamiana* plants of the plant line *FNR:eGFP#7-25* expressing the plastid marker *FNR:eGFP* (Schattat et al., 2011a) were used. Plants were grown in long-day conditions (16-h day and 8-h night) in greenhouse chambers with controlled temperature and humidity. The temperature was approximately 23°C during the day and 19°C at night. Relative humidity was kept around 55%.

Bacterial strains and cultivation

Escherichia coli Top10 cells were used for cloning and DNA propagation. Cells were cultivated at 37°C in LB with the appropriate antibiotic selection. *Agrobacterium* strain GV3101 (pMP90; Koncz and Schell, 1986) was grown in liquid or on solid yeast extract beef (YEB) media containing rifampicin, gentamycin, and either spectinomycin or carbenicillin, while *Xcv* strains were grown in NYG medium supplemented with rifampicin (30°C for both). *Xanthomonas* strains utilized were: *Xcv* 85-10 (wild-type; Thieme et al., 2005), *Xcv* Δ *hrcN* (strain deficient in an ATPase required for type III secretion of effectors; Lorenz and Büttner, 2009 and *Xcv* Δ *xopQ*; Adlung et al., 2016).

Plasmids

For visualization of plastids and stromules, a plastid organelle marker construct was created using the Modular Cloning Toolbox (Weber et al., 2011; Engler et al., 2014). The final construct consisted of the 35S promoter (pICH51277), the chloroplast transit peptide of RUBISCO (SSU in the backbone pICH41258), eGFP (in the backbone pICH41264), and the nopalinsynthase (NOS) terminator (pICH41421), assembled in a Level 1 acceptor plasmid. The *xopQ:mOrange2* expression construct was described previously (Erickson et al., 2018; for more details see Supplemental Materials and Methods S2).

Agrobacterium tumefaciens-mediated transient expression

Plasmids were transformed into *A. tumefaciens* strain GV3101 (pMP90). For transient expression experiments, strains harboring the binary vectors were grown overnight in 5-mL YEB liquid cultures (with appropriate antibiotics), harvested by centrifugation, and resuspended in *Agrobacterium* infiltration medium (10-mM MgCl₂; 5-mM MES, pH 5.6; 0.15- μ M Acetosyringone) with a final optical density (OD_{600nm}) of 0.2. Bacteria harboring the plastid marker and the effector or the mORANGE2 control were mixed in a 1:1 ratio. Using a needleless syringe, bacterial suspensions were inoculated into intercostal areas of the youngest fully expanded leaves of 5- to 6-week-old *N. benthamiana* plants (see Supplemental Materials and Methods S3).

Xcv inoculations

Xcv NYG liquid cultures were centrifuged to harvest cells, bacteria were resuspended in 10-mM MgCl₂, and suspensions were adjusted to an OD_{600nm} of 0.1. All three strains, as well as a buffer control, were then inoculated as described for *A. tumefaciens*. Plastids/stromules were observed at 2 dpi using an epi-fluorescence microscope.

Imaging hardware

For image acquisition, an epi-fluorescence microscope (AxioObserver Z1) setup from Zeiss (Jena, Germany) equipped with an X-Cite fluorescence light source and an MRm monochrome camera (Zeiss, Jena, Germany) was used. GFP fluorescence was recorded using a 38 HE filter cube (Carl

Zeiss AG, Jena, Germany). mORANGE2 fluorescence was recorded utilizing the 43 HE filter cube (Carl Zeiss AG, Jena, Germany). The microscope manufacturer's software (ZenBlue, Zeiss, Germany) controlled image acquisition. All images were captured using a 40x/0.75 NA EC PLAN NEOFLUAR lens.

Imaging procedures and image processing

For the quantification of stromule frequencies, a single leaf disc of each infiltration spot was harvested using a cork borer. Leaf discs were vacuum-infiltrated and mounted on glass slides, and three independent z-stacks of the lower epidermis were collected in transmitted light, eGFP, and mORANGE2 channels. In order to obtain 2D extended depth of field images for quantification, single images of the z-series of each channel were first exported into separate file folders and subsequently combined into single images using software and procedures described in Schattat and Klös gen (2009) (total of three images per disc).

For the quantification of stromule frequencies (SF%), we measured the proportion of plastids with at least one stromule (Erickson et al., 2014). To facilitate the faster quantification of stromule and plastid counts in *N. benthamiana* tissues, we expanded on the previously published MTBCellCounter (Franke et al., 2015) via a ridge detection-based stromule detection algorithm (Möller and Schattat, 2019). The extended MTBCellCounter allows for the detection of plastid bodies as described in Franke et al. (2015) and identifies subsequently plastids with stromules.

The PNAI was described previously (Erickson et al., 2014) and represents the absolute number of plastids in close association with a given nucleus. PNAI was evaluated in the 2D projected images (see image processing). Nuclei were counted as nucleus associated when either the plastid body touched, overlapped with, or was within a distance of 4 µm from the nucleus. Four micrometer corresponds to the average epidermis plastid diameter.

For sample sizes and details on statistical analysis of SF% and PNAI, see Supplemental Materials and Methods S4, Supplemental Tables S1–S5, and Supplemental Statistics S1–S8.

Naming conventions

For conventions used to name mutants, genes, proteins, and artificial DNA constructs, see Supplemental Materials and Methods S5.

Accession numbers

Sequence data from this article can be found in the GenBank/EMBL data libraries under the following accession numbers: AAV74206 (*xopQ*), AAY5460 (*NRG1*), AAL85347 (*EDS1*), Gene ID Niben101Scf02118g00018 (*ADR1*), ATD14363 (*ROG1*), and ABC66096 (*mOrange2*).

Supplemental data

The following materials are available in the online version of this article.

Supplemental Figure S1. Full frames of stacked fluorescence images of a mock and *Xcv* Δ *hrcN* infiltrated FNR:eGFP-7-25 *N. benthamiana* plant.

Supplemental Figure S2. Full frames of stacked fluorescence images of a *Xcv* wild-type and *Xanthomonas campestris* pv. *vesicatoria* Δ *xopQ* infiltrated FNReGFP-7-25 *N. benthamiana* plant.

Supplemental Figure S3. Moderate optical densities of GV3101 (pMP90) induce moderate stromule frequencies at 3 dpi.

Supplemental Figure S4. Full-frame stacked fluorescence images of an *mOrange2* + SSU:eGFP and an *xopQ*:*mOrange2* + SSU:eGFP inoculated *N. benthamiana* wild-type plant.

Supplemental Figure S5. Full-frame stacked fluorescence images of an *mOrange2* + SSU:eGFP and an *xopQ*:*mOrange2* + SSU:eGFP inoculated *N. benthamiana* *roq1* plant.

Supplemental Figure S6. Full-frame stacked fluorescence images of an *mOrange2* + SSU:eGFP and an *xopQ*:*mOrange2* + SSU:eGFP inoculated *N. benthamiana* *eds1* plant.

Supplemental Figure S7. Full-frame stacked fluorescence images of an *mOrange2* + SSU:eGFP and an *xopQ*:*mOrange2* + SSU:eGFP inoculated *N. benthamiana* *nrg1* plant.

Supplemental Figure S8. Macroscopic phenotype, SF%, and PNAI in response to NRG1 over-expression in FNR:eGFP-7-25 transgenic WT plants.

Supplemental Figure S9. Full-frame stacked fluorescence images of an inoculated *N. benthamiana* *adr1_nrg1* plant.

Supplemental Table S1. Summary of SF% values used for stromule frequency bar blots in the main manuscript.

Supplemental Table S2. Summary of PNAI values used for box blots in the main manuscript.

Supplemental Table S3. Values used for SF% bar plots in Supplemental Figure S3A.

Supplemental Table S4. Values used for SF% box plots in Supplemental Figure S8B.

Supplemental Table S5. Values used for PNAI box plots in Supplemental Figure S8D.

Supplemental Statistics S1. For Figure 1 SF.

Supplemental Statistics S2. For Figure 2 SF.

Supplemental Statistics S3. For Figure 3 SF.

Supplemental Statistics S4. For Figure 4 SF.

Supplemental Statistics S5. For Figure 5 SF.

Supplemental Statistics S6. For Figure 6 PNAI.

Supplemental Statistics S7. For Supplemental Figure S3 SF.

Supplemental Statistics S8. For Supplemental Figure S8 SF.

Supplemental Statistics S9. For Supplemental Figure S8 PNAI.

Supplemental Materials and Methods S1. Generation of *Nb nrg1 adr1* double mutant line.

Supplemental Materials and Methods S2. Cloning of plasmids.

Supplemental Materials and Methods S3. Experimental procedure utilized for *A. tumefaciens* infiltration experiments.

Supplemental Materials and Methods S4. Information on sample sizes and data analysis for stromule frequencies and PNAI values.

Supplemental Materials and Methods S5. Naming conventions.

Supplemental References.

Acknowledgments

All *Xcv* strains were kindly provided by Prof. Ulla Bonas, Martin-Luther-Universität Halle-Wittenberg, Germany. Dr. Sebastian Schornack, TSL, Cambridge, UK for advice on the manuscript. We thank Jaqueline Bautor, Junli Wang and Dmitry Lapin (MPIPZ) for help in developing the Cas9-free *adr1_nrg1* double mutant.

Funding

This study was funded by the Deutsche Forschungsgemeinschaft (DFG, German Research Foundation)–400681449/GRK2498, STU642/1-1, and SFB-1403–414786233 as well as Martin-Luther-University core funding.

Conflict of interest statement. There is no conflict of interest.

References

- Adachi H, Contreras M, Harant A, Wu C, Derevnina L, Sakai T, Duggan C, Moratto E, Bozkurt T, Maqbool A, et al. (2019) An N-terminal motif in NLR immune receptors is functionally conserved across distantly related plant species. *eLife* **8**: e49956
- Adlung N, Bonas U (2017) Dissecting virulence function from recognition: cell death suppression in *Nicotiana benthamiana* by XopQ/HopQ1-family effectors relies on EDS1-dependent immunity. *Plant J* **91**: 430–442
- Adlung N, Prochaska H, Thieme S, Banik A, Blüher D, John P, Nagel O, Schulze S, Gantner J, Delker C, et al. (2016) Non-host resistance induced by the *Xanthomonas* effector XopQ is widespread within the genus *Nicotiana* and functionally depends on EDS1. *Front Plant Sci* **7**: 1796
- Bi G, Su M, Li N, Liang Y, Dang S, Xu J, Hu M, Wang J, Zou M, Deng Y, et al. (2021) The ZAR1 resistosome is a calcium-permeable channel triggering plant immune signaling. *Cell* **184**: 3528–3541.e12
- Bonardi V, Tang S, Stallmann A, Roberts M, Cherkis K, Dangl JL (2011) Expanded functions for a family of plant intracellular immune receptors beyond specific recognition of pathogen effectors. *Proc Natl Acad Sci USA* **108**: 16463–16468
- Büttner D (2016) Behind the lines—actions of bacterial type III effector proteins in plant cells. *FEMS Microbiol Rev* **40**: 894–937
- Caplan JL, Kumar AS, Park E, Padmanabhan MS, Hoban K, Modla S, Czymmek K, Dinesh-Kumar SP (2015) Chloroplast stromules function during innate immunity. *Dev Cell* **34**: 45–57
- Castel B, Ngou P-M, Cevik V, Redkar A, Kim D-S, Yang Y, Ding P, Jones JDG (2019) Diverse NLR immune receptors activate defence via the RPW8-NLR NRG1. *New Phytol* **222**: 966–980
- Collier SM, Hamel L-P, Moffett P (2011) Cell death mediated by the N-terminal domains of a unique and highly conserved class of NB-LRR protein. *MPMI* **24**: 918–931
- Cui H, Tsuda K, Parker JE (2015) Effector-triggered immunity: from pathogen perception to robust defense. *Annu Rev Plant Biol* **66**: 487–511
- Delfosse K, Wozny MR, Jaipargas E-A, Barton KA, Anderson C, Mathur J (2016) Fluorescent protein aided insights on plastids and their extensions: a critical appraisal. *Front Plant Sci* **6**: 1233
- Ding X, Jimenez-Gongora T, Krenz B, Lozano-Duran R (2019) Chloroplast clustering around the nucleus is a general response to pathogen perception in *Nicotiana benthamiana*. *Mol Plant Pathol* **8**: 521
- Engler C, Youles M, Gruetzner R, Ehnert T-M, Werner S, Jones JDG, Patron NJ, Marillonnet S (2014) A golden gate modular cloning toolbox for plants. *ACS Synth Biol* **3**: 839–843
- Erickson JL, Adlung N, Lampe C, Bonas U, Schattat MH (2018) The *Xanthomonas* effector XopL uncovers the role of microtubules in stromule extension and dynamics in *Nicotiana benthamiana*. *Plant J* **93**: 856–870
- Erickson JL, Ziegler J, Guevara D, Abel S, Klösgen RB, Mathur J, Rothstein SJ, Schattat MH (2014) *Agrobacterium*-derived cytokinin influences plastid morphology and starch accumulation in *Nicotiana benthamiana* during transient assays. *BMC Plant Biol* **14**: 127–120
- Franke L, Erickson JL, Rödel D, Schröter D, Storbeck B, Möller B, Schattat MH (2015) The “MTB Cell Counter” a versatile tool for the semi-automated quantification of sub-cellular phenotypes in fluorescence microscopy images. A case study on plastids, nuclei and peroxisomes. *Endocytobiosis Cell Res* **26**: 31–42
- Gantner J, Ordon J, Kretschmer C, Guerois R, Stuttmann J (2019) An EDS1-SAG101 complex is essential for TNL-mediated immunity in *Nicotiana benthamiana*. *Plant Cell* **31**: 2456–2474
- Gray JC, Hansen MR, Shaw DJ, Graham K, Dale R, Smallman P, Natesan SKA, Newell CA (2012) Plastid stromules are induced by stress treatments acting through abscisic acid. *Plant J* **69**: 387–398
- Gray JC, Sullivan JA, Hibberd JM, Hansen MR (2001) Stromules: mobile protrusions and interconnections between plastids. *Plant Biol* **3**: 223–233
- Grützner R, Martin P, Horn C, Mortensen S, Cram EJ, Lee-Parsons CWT, Stuttmann J, Marillonnet S (2021) High-efficiency genome editing in plants mediated by a Cas9 gene containing multiple introns. *Plant Commun* **2**: 100135
- Gunning BES (2005) Plastid stromules: video microscopy of their outgrowth, retraction, tensioning, anchoring, branching, bridging, and tip-shedding. *Protoplasma* **225**: 33–42
- Holzinger A, Kwok EY, Hanson MR (2008) Effects of *arc3*, *arc5* and *arc6* mutations on plastid morphology and stromule formation in green and nongreen tissues of *Arabidopsis thaliana*. *Photochem Photobiol* **84**: 1324–1335
- Huang S, Jia A, Song W, Hessler G, Meng Y, Sun Y, Xu L, Laessle H, Jirschitzka J, Ma S, et al. (2022) Identification and receptor mechanism of TIR-catalyzed small molecules in plant immunity. *Science (New York, NY)* **377**: abq3297
- Jacob P, Kim NH, Wu F, Kasmi El F, Chi Y, Walton WG, Furzer OJ, Lietzan AD, Sunil S, Kempthorn K, et al. (2021) Plant “helper” immune receptors are Ca²⁺-permeable nonselective cation channels. *Science (New York, NY)* **373**: 420–425
- Jia A, Huang S, Song W, Wang J, Meng Y, Sun Y, Xu L, Laessle H, Jirschitzka J, Hou J, et al. (2022) TIR-catalyzed ADP-ribosylation reactions produce signaling molecules for plant immunity. *Science (New York, N.Y)* **377**: eabq8180
- Jubic LM, Saile S, Furzer OJ, Kasmi El F, Dangl JL (2019) Help wanted: helper NLRs and plant immune responses. *Curr Opin Plant Biol* **50**: 82–94
- Koncz C, Schell J (1986) The promoter of T-L-DNA gene 5 controls the tissue-specific expression of chimaeric genes carried by a novel type of *Agrobacterium* binary vector. **204**: 383–396
- Köhler RH, Hanson MR (2000) Plastid tubules of higher plants are tissue-specific and developmentally regulated. *J Cell Sci* **113** (Pt 1): 81–89
- Krenz B, Jeske H, Kleinow T (2012) The induction of stromule formation by a plant DNA-virus in epidermal leaf tissues suggests a novel intra- and intercellular macromolecular trafficking route. *Front Plant Sci* **3**: 291

- Kretschmer M, Damoo D, Djamei A, Kronstad J** (2020) Chloroplasts and Plant Immunity: Where Are the Fungal Effectors? *Pathogens* **9**: 19
- Kumar AS, Park E, Nedo A, Alqarni A, Ren L, Hoban K, Modla S, McDonald JH, Kambhamettu C, Dinesh-Kumar SP, et al.** (2018) Stromule extension along microtubules coordinated with actin-mediated anchoring guides perinuclear chloroplast movement during innate immunity. *eLife* **7**: e23625
- Lapin D, Bhandari DD, Parker JE** (2020) Origins and immunity networking functions of EDS1 family proteins. *Annu Rev Phytopathol* **58**: 253–276
- Lapin D, Kovacova V, Sun X, Dongus JA, Bhandari D, Born von P, Bautor J, Guarneri N, Rzemieniewski J, Stuttmann J, et al.** (2019) A coevolved EDS1-SAG101-NRG1 module mediates cell death signaling by TIR-domain immune receptors. *Plant Cell* **31**: 2430–2455
- Lorenz C, Büttner D** (2009) Functional characterization of the type III secretion ATPase HrcN from the plant pathogen *Xanthomonas campestris* pv. *vesicatoria*. *J Bacteriol* **191**: 1414–1428
- Lu Y, Tsuda K** (2021) Intimate association of PRR- and NLR-mediated signaling in plant immunity. *MPMI* **34**: 3–14
- Ma S, Lapin D, Liu L, Sun Y, Song W, Zhang X, Logemann E, Yu D, Wang J, Jirschitzka J, et al.** (2020) Direct pathogen-induced assembly of an NLR immune receptor complex to form a holoenzyme. *Science (New York, NY)* **370**: eabe3069
- Martin R, Qi T, Zhang H, Liu F, King M, Toth C, Nogales E, Staskawicz BJ** (2020) Structure of the activated ROQ1 resistosome directly recognizing the pathogen effector XopQ. *Science (New York, NY)* **370**: eabd9993
- Mathur J, Mammone A, Barton KA** (2012) Organelle extensions in plant cells. *J Integr Plant Biol* **54**: 851–867
- Möller B, Schattat MH** (2019) Quantification of stromule frequencies in microscope images of plastids combining ridge detection and geometric criteria. In *Proceedings of the 12th International Joint Conference on Biomedical Engineering Systems and Technologies (BIOSTEC 2019)*, Vol. 2: BIOIMAGING. INSTICC, SciTePress, Prague, Czech Republic, pp. 38–48
- Mullineaux PM, Selga T, Selga M, Exposito-Rodríguez M, Laissue PP, Gobiňš V, Smirnov N, Laser AO, Park E** (2020) Spatial chloroplast-to-nucleus signalling involving plastid-nuclear complexes and stromules. *Philos Trans R Soc Lond B Biol Sci* **375**: 20190405
- Ngou BPM, Ahn H-K, Ding P, Redkar A, Brown H, Ma Y, Youles M, Tomlinson L, Jones JDG** (2020) Estradiol-inducible AvrRps4 expression reveals distinct properties of TIR-NLR-mediated effector-triggered immunity. *J Exp Bot* **71**: 2186–2197
- Ordon J, Gantner J, Kemna J, Schwalgun L, Reschke M, Streubel J, Boch J, Stuttmann J** (2017) Generation of chromosomal deletions in dicotyledonous plants employing a user-friendly genome editing toolkit. *Plant J* **89**: 155–168
- Ordon J, Martin P, Erickson JL, Ferik F, Balcke G, Bonas U, Stuttmann J** (2021) Disentangling cause and consequence: genetic dissection of the DANGEROUS MIX2 risk locus, and activation of the DM2h NLR in autoimmunity. *Plant J* **106**: 1008–1023
- Pruitt RN, Locci F, Wanke F, Zhang L, Saile SC, Joe A, Karelina D, Hua C, Fröhlich K, Wan W-L, et al.** (2021) The EDS1-PAD4-ADR1 node mediates Arabidopsis pattern-triggered immunity. *Nature* **598**: 495–499
- Pyke KA** (2013) Divide and shape: an endosymbiont in action. *Planta* **237**: 381–387
- Qi T, Seong K, Thomazella DPT, Kim JR, Pham J, Seo E, Cho M-J, Schultink A, Staskawicz BJ** (2018) NRG1 functions downstream of EDS1 to regulate TIR-NLR-mediated plant immunity in *Nicotiana benthamiana*. *Proc Natl Acad Sci USA* **115**: E10979–E10987
- Saile SC, Jacob P, Castel B, Jubic LM, Salas-González I, Bäcker M, Jones JDG, Dangl JL, El Kasmi F** (2020) Two unequally redundant “helper” immune receptor families mediate Arabidopsis thaliana intracellular “sensor” immune receptor functions. *PLoS Biol* **18**: e3000783
- Schattat M, Barton K, Baudisch B, Klösgen RB, Mathur J** (2011a) Plastid stromule branching coincides with contiguous endoplasmic reticulum dynamics. *Plant Physiol* **155**: 1667–1677
- Schattat MH, Klösgen RB** (2009) Improvement of plant cell microscope images by use of “depth of field” extending software. *Endocytobiosis Cell Res* **19**: 11–19
- Schattat MH, Klösgen RB** (2011b) Induction of stromule formation by extracellular sucrose and glucose in epidermal leaf tissue of *Arabidopsis thaliana*. *BMC Plant Biol* **11**: 115
- Schultink A, Qi T, Lee A, Steinbrenner AD, Staskawicz B** (2017) Roq1 mediates recognition of the *Xanthomonas* and *Pseudomonas* effector proteins XopQ and HopQ1. *Plant J* **92**: 787–795
- Sheahan MB, Collings DA, Rose RJ, McCurdy DW** (2020) ACTIN7 is required for perinuclear clustering of chloroplasts during Arabidopsis protoplast culture. *Plants* **9**: 225
- Sheahan MB, Rose RJ, McCurdy DW** (2004) Organelle inheritance in plant cell division: the actin cytoskeleton is required for unbiased inheritance of chloroplasts, mitochondria and endoplasmic reticulum in dividing protoplasts. *Plant J* **37**: 379–390
- Stuttmann J, Barthel K, Martin P, Ordon J, Erickson JL, Herr R, Ferik F, Kretschmer C, Berner T, Keilwagen J, et al.** (2021) Highly efficient multiplex editing: one-shot generation of 8 × *Nicotiana benthamiana* and 12 × *Arabidopsis* mutants. *Plant J* **106**: 8–22
- Sun X, Lapin D, Feehan JM, Stolze SC, Kramer K, Dongus JA, Rzemieniewski J, Blanvillain-Baufumé S, Harzen A, Bautor J, et al.** (2021) Pathogen effector recognition-dependent association of NRG1 with EDS1 and SAG101 in TNL receptor immunity. *Nat Commun* **12**: 3335–3315
- Teper D, Burstein D, Salomon D, Gershovitz M, Pupko T, Sessa G** (2016) Identification of novel *Xanthomonas euvesicatoria* type III effector proteins by a machine-learning approach. *Mol Plant Pathol* **17**: 398–411
- Thieme F, Koebnik R, Bekel T, Berger C, Boch J, Büttner D, Caldana C, Gaigalat L, Goesmann A, Kay S, et al.** (2005) Insights into genome plasticity and pathogenicity of the plant pathogenic bacterium *Xanthomonas campestris* pv. *vesicatoria* revealed by the complete genome sequence. *J Bacteriol* **187**: 7254–7266
- Tian H, Wu Z, Chen S, Ao K, Huang W, Yaghmaiean H, Sun T, Xu F, Zhang Y, Wang S, et al.** (2021) Activation of TIR signalling boosts pattern-triggered immunity. *Nature* **598**: 500
- Toruño TY, Stergiopoulos I, Coaker G** (2016) Plant-pathogen effectors: cellular probes interfering with plant defenses in spatial and temporal manners. *Annu Rev Phytopathol* **54**: 419–441
- Vismans G, van der Meer T, Langevoort O, Schreuder M, Bouwmeester H, Peisker H, Dörman P, Ketelaar T, van der Krol A** (2016) Low-phosphate induction of plastidial stromules is dependent on strigolactones but not on the canonical strigolactone signaling component MAX2. *Plant Physiol* **172**: 2235–2244
- Wagner S, Stuttmann J, Rietz S, Guerois R, Brunstein E, Bautor J, Niefind K, Parker JE** (2013) Structural basis for signaling by exclusive EDS1 heteromeric complexes with SAG101 or PAD4 in plant innate immunity. *Cell Host Microbe* **14**: 619–630
- Wang J, Hu M, Wang J, Qi J, Han Z, Wang G, Qi Y, Wang H-W, Zhou J-M, Chai J** (2019a) Reconstitution and structure of a plant NLR resistosome conferring immunity. *Science (New York, NY)*. doi: [10.1126/science.aav5870](https://doi.org/10.1126/science.aav5870)
- Wang J, Wang J, Hu M, Wu S, Qi J, Wang G, Han Z, Qi Y, Gao N, Wang H-W, et al.** (2019b) Ligand-triggered allosteric ADP release primes a plant NLR complex. *Science (New York, NY)*. doi: [10.1126/science.aav5868](https://doi.org/10.1126/science.aav5868)
- Weber E, Engler C, Gruetzner R, Werner S, Marillonnet S** (2011) A modular cloning system for standardized assembly of multigene constructs. *PLoS ONE* **6**: e16765
- Wu Z, Li, M Dong, OX Xia, S Liang, W Bao, Y Wasteneys, GLi X** (2019) Differential regulation of TNL-mediated immune signaling by redundant helper CNLs. *New Phytol* **222**: 938–953
- Yuan M, Ngou BPM, Ding P, Xin X-F** (2021) PTI-ETI crosstalk: an integrative view of plant immunity. *Curr Opin Plant Biol* **62**: 102030